GLL

ASSESSMENT OF RELATIVE-ACTIVE TECTONICS IN RHUMEL-SMENDOU BASIN (NE ALGERIA) – OBSERVATIONS FROM THE MORPHOMETRIC INDICES AND HYDROGRAPHIC FEATURES OBTAINED BY THE DIGITAL ELEVATION MODEL

Nabil Manchar, Riheb Hadji, Ahmed Bougherara, Kamel Boufaa

Summary

The eastern Tell Atlas of Algeria is characterized by a complex neotectonic system including lateral strike-slips, and normal and reverse faults. The landscape of the Neogene basin of Mila-Constantine acquired its shape due to the perpetual action of tectonic activity, and erosion processes. Neo-tectonics in this basin have affected the geometry of the stream network and the contemporary landscape topography. Our methodology evaluates the active tectonics in this mountainous region by a combination of drainage network and geomorphic indices, namely, the basin-shape index (Bs), stream-length gradient (SL), hypsometric integral (HI), mountain front sinuosity (Smf), basin asymmetry factor (AF), and valley-floor ratio (Vf). The calculated values of the six measured geomorphic indices were used to differentiate the distribution of faults function as well as the relative tectonic activity in the study area. The obtained results from the GIS-based multi-criteria analysis of these indices consist of the index of active tectonics (IAT). Hence, we defined four hierarchic degrees of IAT, namely, very high (VH), high (H), moderate (M), and low (L). The relative active tectonics represents an obvious correlation between morpho-structural features, tectonic activities, and uplift rates. It selects the morphotectonic features and landforms that interpret the tectonic events in the study area. Our results prove that this approach discerns the most active regions related to the neo-tectonic action in the Rhumel-Smendou drainage basin. The combination of geomatics and field surveys highlights the cliffs which are still rising by using the drainage patterns, the landform model, and the mountain range shape.

Keywords

Bs • SL • Hi • Smf • AF • Vf • IAT

1. Introduction

The NNW-SSE convergence between the Nubian and Eurasian plates is responsible for the recent tectonic activity in northern Africa. This activity was initiated in the

Late Cretaceous [McKenzie 1972]. The Maghrebides Belt in the Western and Central Mediterranean accumulates 3–6 mm yr-1 of crustal shortening, dextral shearing, and 2.4 mm yr-1 on the Guelma E-W- trending lateral strike-slip [Bougrine et al. 2019], presenting, thus, a major structural seismotectonic element in the region [Bendjama et al. 2021]. Neogene and Quaternary post-nape basins contain a series of E-W to NE-SW trending folds associated with active faults [Meghraoui 1988].

Neotectonics is the upper Tertiary and the Quaternary tectonic movements have influenced the current shape of the relief. The neotectonic activity associated with continental uplift stands out along the meridional border of Numidic Chain by faults scarps, deeply incised rivers, and filling deposits along mountain fronts and in fault-bounded valleys [Benabbas 2006, Hadji et al. 2013, 2014, Manchar et al. 2018, 2019]. The North range of Algeria has undergone septentrional structuring in result of the convergence of Nubian and Eurasian plates. Despite extensive research on the morphotectonics of the Algerian alpine chain, little is known about the tectonics of the Neogene basin of Constantine. In the last decades, the sequent seismic events have demonstrated that this region is strongly influenced by a compressive geodynamic action [Benouar 1994, Harbi et al. 2003, Mahleb et al. 2022].

The quantitative and qualitative assessment of seismic activity requires the evaluation of the Holocene and Pleistocene dynamic tectonics [Keller and Pinter 2002]. Recently, several researchers have studied the Tellian Atlas in Northeast Algeria [Yelles-Chaouache et al. 2006]. The tectonic geochronology of an area can be correlated with the spatial combination of different morphotectonic indices, measured in a field survey and derived from topographic maps, aerial photographs digital elevation models, and satellite data [Keller 1986]. The GIS-multicriteria analysis allows to assess the dynamics of river evolution and the characteristics of the drainage shape related to the morpho-structural and neotectonic evolution in the study area. This technique was widely used by several researchers in natural hazard assessment [Keller and Pinter 1996, Hadji et al. 2014, Zahri et al. 2016, Dahoua et al. 2017, Mouici et al. 2017, El Mekki et al. 2017, Rais et al. 2017, Anis et al. 2019, Ncibi et al. 2020]. The disastrous seismic event that occurred in Mila town on August 07th, 2020, with a magnitude of 4.9 degrees induced several landslides which damaged the urban sites in the western parts of Mila (Fig. 1a). Tectono-structural and geomorphologic framework prospection together with specific geophysical and geotechnical tests are necessary to understand the causes of the landslides and the evaluation of the current state of the damaged sites, as well as to propose a model of landslide behavior in the Rhumel-Smendou Neogene basin. The main aim of our paper is to delineate/rate the active tectonics areas based on geomorphic indices, namely, the stream gradient (*SL*), drainage basin asymmetry (*AF*), and basin shape (*Bs*), hypsometric integral (*Hi*) along with convex-up hypsometric curve, valley floor width-valley height ratio (*Vf*), drainage basin shape such as mountain-front sinuosity (*Smf*). Thereby, the fault structures that might have been responsible for the active tectonics and the earthquake sequences have been highlighted. Therefore, the relationships between these events and local faults are established by integrating the geological and seismo-tectonic data. By consulting the geo-scientific literature, we have

found that the geomorphic indices and the drainage patterns had been widely used in evaluating neotectonic activities worldwide [Wells et al. 1988, Azor et al. 2002]. Bull and McFadden [1977] and Silva et al. [2003] have linked the VF, Smf, and BS indexes to evaluate tectonic activity. Whereas, El-Hamdouni et al. [2008] developed and applied a model that included the *Af*, *Hi*, *SL*, *VF*, *Smf, and Bs*, indices. Thus, the aim of this research was to introduce a combined approach that will be useful in showing relative active tectonic events of an area by applying geomorphic indices and drainage patterns.

Our approach follows three main phases: 1) the evaluation of the geomorphic indices and the drainage patterns, *ii*) the calibration of six geomorphic indices, and 2) the calculation and the classification of IAT index. This study demonstrates the usefulness of this kind of methods of assessing the neotectonic activity in the Neogene basins of Mediterranean countries. Our result would help decision-makers and academic researchers to mitigate geologic hazards that could affect the great dam of Beni Haroun and megalopolis of Constantine.

2. General setting

The Rhumel-Smendou (1081.28 km³; longitude of 249641 to 302110 E; and latitude of 4021372 to 4051694 N, WGS 84, UTM 32N) is a sub-watershed of the great Kebir-Rhumel basin. It was structured during the Tertiary period in result of the evolution of the Tellian-Atlasic chain [Benabbas 2006, Tamani et al. 2019] (Fig. 1b).
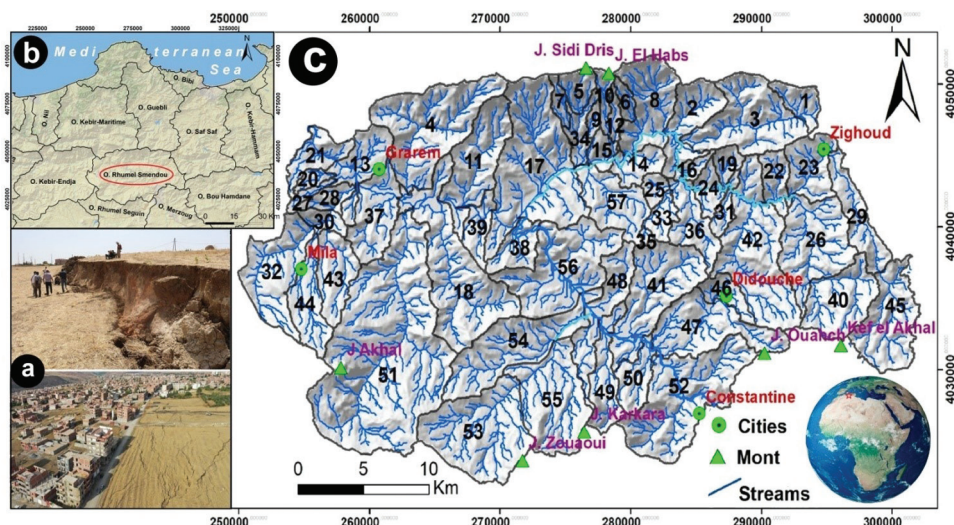
Source: Authors' own study

Fig. 1. a) Photos of the mega-Landslides caused by the seism of Mila 07/08/20 (Mw = 4.9). b) Geographic location of the study area. c) the 57 sub-basins of the Rhumel-Smendou basin

This basin was filled by a silico-clastic and carbonatic series of Mio-plio-quaternary age, installed on a substratum that was pre-structured by thrust sheet units of the Tellian, Penitellian, and neritic units belonging to the external zones of eastern Algeria Maghrebian chain [Wildi 1983, Coiffait 1992, Hamad et al. 2018]. The altitude ranges from 500 to 1350 m a.s.l.

This area is characterized by a well-developed stream network, including Bouhadjeb, El Kram, El Aria, and Smendou wadi, which are the main watercourse of the basin (Fig. 1c). All these wades flow toward the Northeast [Hamed et al. 2017]. The study area is characterized by a semi-arid climate, with a dry and hot summer, and humid and cold winter [Demdoum et al. 2015]. Precipitations range from 600 to 900 mm/year; most of rain falls between Decembers to February [Benmarce et al. 2021]. The study area could be subdivided into three distinct natural sub-areas: the first one is the mountainous massifs of the Numidian chain in the north, the second is the hills of Smendou and Zardezas with altitudes varying from 400 to 500 m a.s.l. and the third is the valley areas including the depression of Beni Brahim-BouHadjeb and the Smendou valley. The morphology shows three units: Ouled Kebbeb, Smendou (which is analyzed in this paper), and Mila (which remains the most important). These units are inserted between the Numidian chain in the north and the mountains of Constantine in the south. Geologically, the study area is characterized by the superposition of thrust sheet units made up from the base to the top by: Neritic unit (Cretaceous carbonate), Ultra-Tellian unit (Cretaceous-Eocene marls and marly limestone), Tellian units: Marly dominance (Cretaceous-Eocene), Numidian unit with sandstone Burdigalian, clay, and flysch (Eocene), Mio-Plio-Quaternary: sandy clays, marls, and conglomerate (Mio-Pliocene). Alluvial terraces and lacustrine calcareous formations from the Quaternary period [Raoult 1974, Coiffait and Vila 1977, Vila 1980]. This structure was deposited during the paroxysmal compressional phases of the Eocene and Miocene (Fig. 2a) [Guiraud 1973, Durand-Delga 1969].

3. Material and methods

3.1. Data sources

This research uses a 30-m resolution digital elevation model (SRTM/DEM) and 1/25000 topographic maps for the generation of the stream network and the derivation of morphometric indices. Six 1/50000 geological maps were used, namely, of Sidi Merouane N° 50, Sidi Driss N° 51, Zighoud Youcef N° 52, Radjas N° 72, Constantine N° 73, and El Aria N° 74, for the structural study and lithological identification (Fig. 2b). Therefore, field surveys and satellite imagery (data ETM+ Landsat 8) observations were drawn on for a detailed analysis of the study area. The Arcgis 10.8 software was run to create and process the Geodatabase. The stream network was extracted and sub-watersheds were delineated using multiple flow direction algorithms. Hence fifty-seven drainage sub-basins were identified (Table 1) (Fig. 1c). The adopted approach is resumed in the methodological flowchart of the Figure 3.
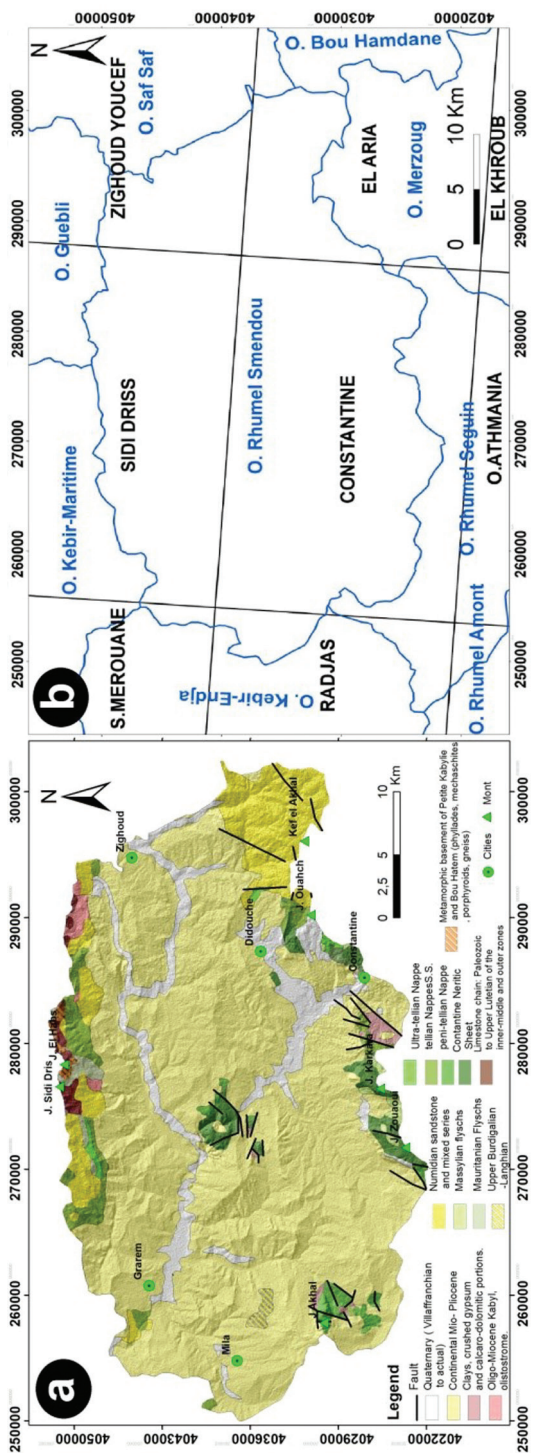
Source: Authors' own study

Fig. 2. a) geological map of the study area. b) the drainage basins on the 1/50000 cartogram
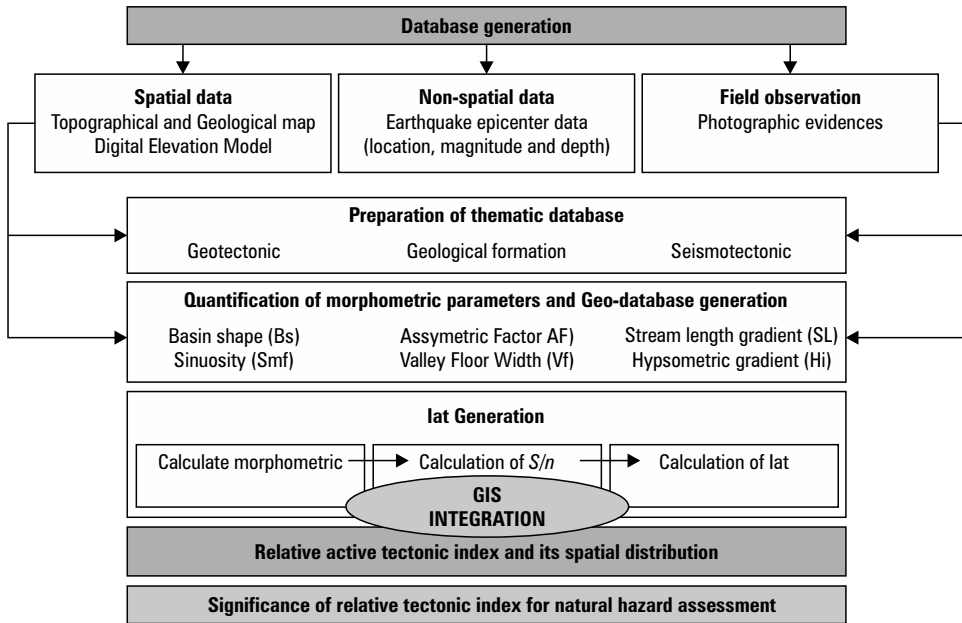
Source: Authors' own study

Fig. 3. Methodological flowchart of the adopted approach

3.2. Calculation of geomorphic indices

Basin shape index (*Bs*)

Drainage basins tend to take on an elongated shape in active tectonic areas. Thus, high values of *Bs* are typically associated with elongated basins, whereas low values indicate circular basins. *Bs* is calculated by the eq. (1):

$$Bs = B_l/B_w \tag{1}$$

While B_l is the length between the headwaters and the mouth of the basin, B_w is the width of the basin measured at its widest point [Ramírez-Herrera 1998].

Stream-length gradient index (*SL*)

Rivers typically acquire smooth concave longitudinal profiles [Snow and Slingerland 1987]. Anomalously high SL values highlight tectonics activity [Keller 1986]. Hence, perturbations in river profiles may be explained as a reaction to continuous tectonism. SL is calculated by the eq. (2):

$$SL = \Delta H/\Delta L \cdot L \tag{2}$$

where: $\Delta H/\Delta L$ is the channel slope or gradient of the reach, and L is the total channel length.

Hypsometric integrals (*Hi*)

Hypsometric curves and hypsometric integrals are important to understand drainage basin development caused by its erosional and depositional activities [El Hamdouni et al. 2008]. *Hi* is calculated by the eq. (3):

$$Hi = (Elev_{avg} - Eleva_{min})/(Elev_{max} - Elev_{min}) \tag{3}$$

where: $Elev_{avg}$, $Elev_{min}$ and $Elev_{max}$ are the average, lowest, and highest elevations.

Mountain front sinuosity index (*Smf*)

The mountain front sinuosity index has been defined by (Bull 1978). *Smf* is calculated by the eq. (4):

$$Smf = Lmf / Ls \tag{4}$$

where: L_{mf} and *Ls* are, respectively, the planimetric length and the length of a mountain front measured in a straight line.

Asymmetry factor (*AF*)

Asymmetry factor (*AF*) is a significant tool in determining the tectonic tilting of the basin. An *AF* value above or below 50 may result from basin tilting, resulting either from active tectonics or structural control differential erosion [Hare and Gardner 1985]. *AF* is calculated by the eq. (5):

$$AF = (A_r/A_t) \cdot 100 \tag{5}$$

where: A_r and A_t are, respectively, the area of the right side of the main channel facing downstream and the total area of the basin.

Valley floor (*Vf*)

Vf is defined as the ratio of the width of the valley floor to its average height [Bull 1978]. *Vf* is calculated by the eq. (6):

$$Vf = 2Vf_w / [(E_{ld} - E_{sc}) + (E_{rd} - E_{sc})] \tag{6}$$

where:
- Vf – the ratio of valley floor width to valley height,
- Vf_w – the width of the valley floor,
- E_{ld} – the elevation of the divide on the left side of the valley,
- E_{rd} – the elevation on the right side,
- E_{sc} – the average elevation of the valley floor.
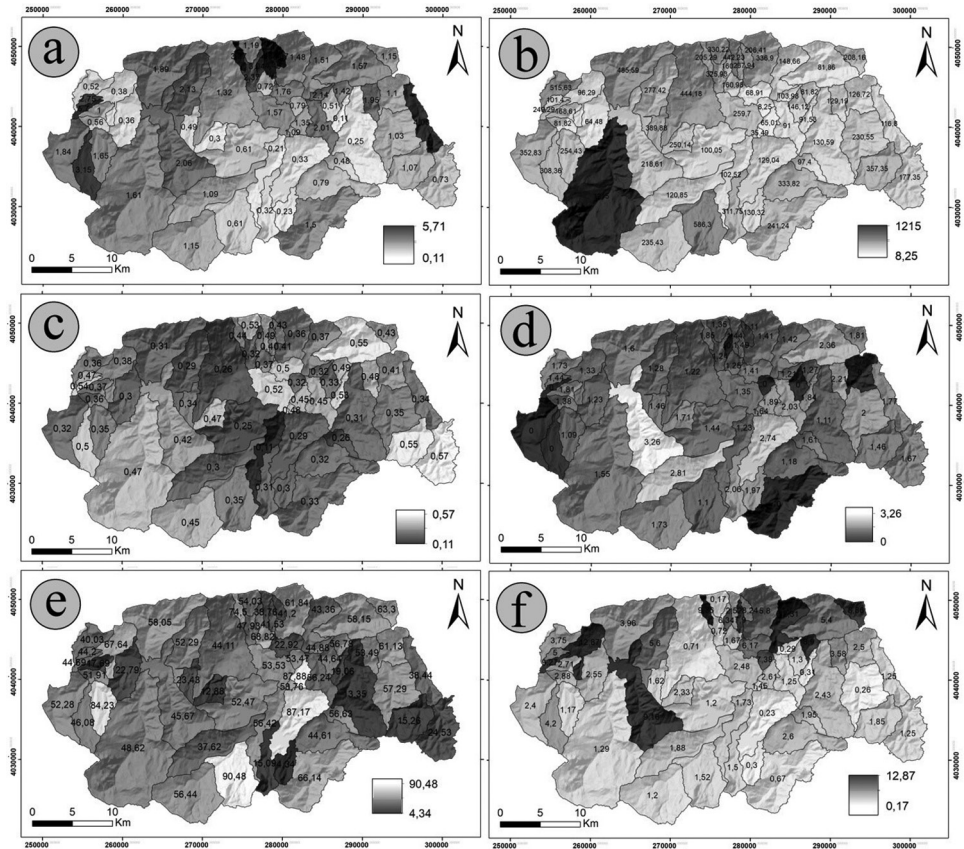
Source: Authors' own study

Fig. 4. Values of geomorphic indices: a) *Bs*. b) *SL*. c) *Hi*. d) *Smf*. e) *Af*. f) *Vf*

4. Results and discussions

We have determined the geomorphic indices in order to analyze topography, drainage network and the role of relative active tectonic in the deformational process. The geomorphic indices are determined for all 57 basins (Table 1).

- *Bs* values of the 57 basins range from 0.11 to 5.71 (Fig. 4a). The NW border of Rhumel-Smendou basin gives the highest values; whereas, the lowest ones appear along the Rhumel watercourse. *Bs* values are ranked into 3 classes, namely: Class 1 (> 4); Class 2 (4–3) and Class 3 (< 3) (Fig. 5a).
- *SL* values for the Rhumel river are ranging from 1215 to 8.25 (Fig. 4b), which generally infer that high SL values occur in the areas where active tectonics has resulted in vertical deformation at the earth's crust (Fig. 5b). The comparison of the lower knickpoint with SL anomalous value demonstrates that the study area is dominated

by active faults signatures such as the Rhumel river showing tremendous lateral shifts and meanders in this reach, preserved several braided bar deposits, developing new terrace scarps, etc.

- *Hi* values on the higher side of *Hi* indicate the formation of landforms due to active tectonics. The hypsometric curves of all the basins are cumulatively analysed to represent young, mature and old stages of the basins' development. The Hi values vary between 0.11 (basin 48) to 0.57 (basin 45) (Fig. 4c). All values are ranked into three classes, namely: Class 1 (> 0.5) of convex hypsometric curves, Class 2 (0.4–0.5) of concave-convex hypsometric curves and Class 3 (< 0.4) of concave hypsometric curves (Fig. 5c).
- *Smf* values linked between the mountain fronts and active tectonics. The active uplift is straight with low values of *Smf*. The values of this index range from 1,1 to 3,26 (Fig. 4d). The lowest values are associated with the SW border of the Rhumel-Smendou sub-watershed (Fig. 5d).
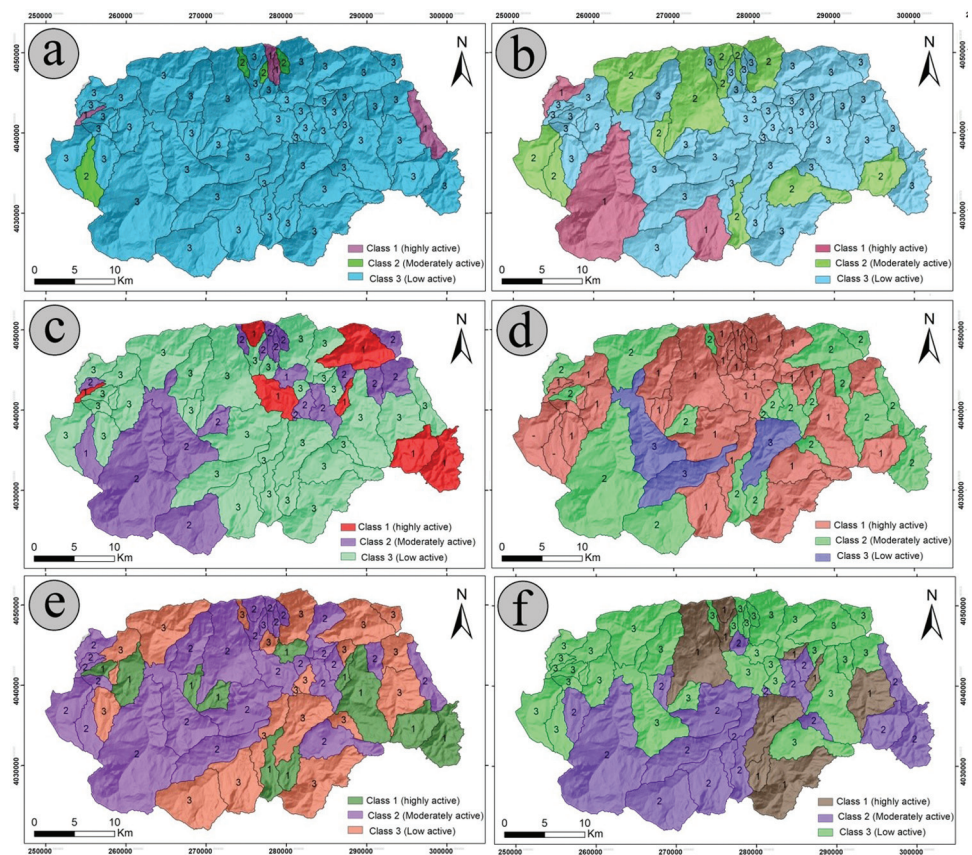
Source: Authors' own study

Fig. 5. Classes of geomorphic indices: a) *Bs*. b) *SL*. c) *Hi*. d) *Smf*. e) *Af*. f) *Vf*

- *AF* value close to 50 signals a slight tilting that is perpendicular to the stream flow. The arrow indicates an asymmetry direction of the basins. AF values are divided into three classes, namely: Class 1 (> 15), Class 2 (7–5), and Class 3 (< 7). Basin N° 55 with the highest AF value is an asymmetrical basin, while basin N° 4 with the lowest value proves to be a gently asymmetric basin. Class 1 denotes fully asymmetrical basins with values ranging from 16,14 to 40,48, while Class 2 and 3 indicate gently asymmetric basins with values ranging from 7,29 to 13,30 for Class 2, and 6,78 to –45,66 for Class 3 (Fig. 4 e, 5e). In this study, the basins that belong to the Class 1 correspond to the SE of the subwatershed and the W border. The high tectonically activity zone covers an area of 270.4 km².
- *Vf* values of the main 164 streams range from 0.17 (basin N° 5) to 12.87 (basin N° 13) (Fig. 4 f). *Vf* has been sorted into three classes: Class 1 (< 1), Class 2 (1–2), and Class 3 (> 2) (Fig. 5 f). The valley floor width to valley height ratio indicates a V-shape with low values and U-shape with higher values of *Vf*. V-shape valley represents a young stage of basin development. The faults passing from V-shaped valleys undergo more intensive erosional processes, and these basins show landslide activity.

Tectonic activity based on geomorphic indices and seismic activity

This study presents data on geomorphic indices that have been already used in other studies to estimate landscape in terms of potential tectonic activity. Overall, the indices are discussed in relation to a particular area, and assessed in regard to relative tectonic activity [Bull and McFadden 1977, Rockwell et al. 1985]. The method presented in this study is adopted to evaluate an index over an area that represents relative tectonic activity (*Iat*).

Several studies have used a combination of two indices (*Smf* and *Vf*) to provide semi-quantitative information on the relative degree of tectonic activity of mountain fronts. Previous studies using these indices provide a classification of tectonic activity [Silva et al. 2003]. It suggests that V-shaped valleys with low *Vf* values < 1 develop in response to active uplift, and that the broad U-shaped valleys with high *Vf* values > 1 indicate significant lateral erosion, due to the absence of tectonic activity. In some studies, the morphometric analysis includes integrating *Vf* and *Smf* values, such as frequency distribution diagrams, showing the distribution of these values along streams and along the mountain front. *Vf* values are overlaid with *Smf* values on the same diagram to give a better picture of the relative degree of tectonic activity and to recognize three different classes. These authors describe 'active fronts' by low values of *Smf* (< 1.6) and *Vf* (< 0.5) indices, characterized by the presence of steep alluvial fans receiving Holocene sediments at the apex, triggered by uplift rates of the order of 1 to 5 m/ka. Rockwell et al. [1985] suggest that lower uplift rates of 0.4 to 0.5 m/ka were sufficient to maintain *Smf* values at 1.4 and *Vf* values at 1, and thus generate active fronts (class 1). They also reported that alluvial fans and gullies can develop along active fronts. These studies focused on the assessment of active tectonics along mountain fronts, ignoring the regional assessment. El Hamdouni [2008] presented a method for the evaluation by an index of an area that represents tectonic activity by arbitrarily dividing various indices

**Table 1.** Values and classifications of *Bs, SL, Hi, Smf, Af, Vf,* and *Iat*

N°	Name	Area (km²)	Bs Value	Bs Class	SL Value	SL Class	Hi Value	Hi Class	Smf Value	Smf Class	Af Value	Af Class	Vf Value	Vf Class	S/n	Iat	Cclass
1	J Bit_Edjazia	7.06	1.15	3	208.16	3	0.43	2	1.81	2	63.3	3	8.86	3	2.67	2.67	4
2	J Rara	16.85	1.51	3	148.66	3	0.37	3	1.42	1	43.36	2	12.31	3	2.50	2.50	4
3	J Souari	32.27	1.57	3	81.86	3	0.55	1	2.36	2	58.15	3	5.4	3	2.50	2.50	4
4	J Bounouara	42.23	1.89	3	485.59	2	0.31	3	1.6	2	58.05	3	3.96	3	2.67	2.67	4
5	K Sidi Dris	6.14	1.19	3	330.22	2	0.53	1	1.35	1	54.03	2	0.17	1	1.67	1.67	2
6	J Habs	3.04	3.67	2	206.41	3	0.43	2	1.11	1	41.2	2	3.24	3	2.17	2.17	3
7	Merdj Guettar	3.24	3.37	2	205.29	3	0.44	2	1.85	2	74.5	3	9.36	3	2.50	2.50	4
8	Echabia	22.66	1.48	3	336.9	2	0.36	3	1.41	2	61.84	3	5.8	3	2.67	2.67	4
9	Kt Nachou	2.06	3.05	2	160.00	3	0.4	2	–	–	53.32	3	6.34	3	2.17	2.17	3
10	J Essafia	4.04	4.80	1	442.23	2	0.49	2	1.44	1	38.76	2	2.52	3	1.83	1.83	2
11	El Khanga	26.07	2.13	3	277.42	3	0.29	3	1.28	1	52.29	2	5.6	3	2.50	2.50	4
12	Mt El Marra	2.83	4.49	1	267.94	3	0.41	2	1.49	1	41.53	2	7.9	3	2.00	2.00	3
13	Grarem	14.56	0.38	3	96.29	3	0.38	3	1.33	1	67.64	3	12.87	3	2.67	2.67	4
14	Takouk	8.20	1.76	3	68.91	3	0.5	1	1.41	1	22.92	1	6.17	3	2.00	2.00	3
15	Mt el Hamri	4.71	0.72	3	160.98	3	0.37	3	1.25	1	68.82	3	1.67	2	2.50	2.50	4
16	Ain Safsafa	3.16	2.14	3	103.98	3	0.32	3	1.21	1	44.88	2	0.29	1	2.17	2.17	3
17	Hammam	55.69	1.33	3	444.18	2	0.26	3	1.22	1	44.11	2	0.71	1	2.00	2.00	3
18	El Malha	47.20	2.07	3	218.61	3	0.42	2	3.26	3	45.67	2	9.16	3	2.67	2.67	4

Table 1. cont.

N°	Name	Area (km²)	Bs Value	Bs Class	SL Value	SL Class	Hi Value	Hi Class	Smf Value	Smf Class	Af Value	Af Class	Vf Value	Vf Class	S/n	Iat	Class
19	Ct Zafrane	4.59	1.42	3	81.82	3	0.49	2	1.27	1	56.78	3	8.9	3	2.50	2.50	4
20	D^{ouar} Ferdoua	2.76	2.75	3	101.40	3	0.47	2	1.44	1	44.2	2	5	3	2.33	2.33	3
21	S^{idi} Merouane	10.30	0.52	3	515.63	1	0.36	3	1.73	2	40.03	2	3.75	3	2.33	2.33	3
22	Smendou^{East}	7.96	1.95	3	129.19	3	0.48	2	2.21	2	53.49	2	3.58	3	2.50	2.50	4
23	Zighoud Y	14.82	1.10	3	126.72	3	0.41	2	–	–	61.13	3	2.5	3	2.33	2.33	3
24	Smendou	6.09	0.52	3	146.12	3	0.33	3	–	–	44.64	2	1.3	2	2.17	2.17	3
25	Cht Bt Merdja	3.67	0.80	3	08.25	3	0.32	3	–	–	53.47	2	7.38	3	2.33	2.33	3
26	Bj Benzekri	29.89	1.04	3	230.55	3	0.35	3	2	2	57.29	3	0.26	1	2.50	2.50	4
27	S^{idi} Merouane1	2.46	5.71	1	249.29	3	0.54	1	–	–	44.69	2	9.27	3	1.67	1.67	2
28	Mt Ain Foul	5.17	1.00	3	168.61	3	0.37	3	1.81	2	17.69	1	2.71	3	2.50	2.50	4
29	J Enadour	14.89	4.03	1	116.8	3	0.34	3	1.77	2	38.44	2	1.25	2	2.17	2.17	3
30	Mat Fellaga	4.64	0.57	3	81.82	3	0.36	3	1.38	1	51.91	2	2.88	3	2.50	2.50	4
31	Bled Mestina	4.40	0.11	3	91.53	3	0.53	1	1.84	2	19.06	1	0.31	1	1.83	1.83	2
32	Mila	25.93	1.85	3	352.83	2	0.32	3	–	–	52.28	2	2.4	3	2.17	2.17	3
33	B Ouegguet	5.44	1.35	3	65.01	3	0.45	2	1.89	2	87.88	3	2.61	3	2.67	2.67	4
34	Bablehmar	6.38	2.37	3	325.93	2	0.32	3	1.24	1	47.93	2	0.72	1	2.00	2.00	3
35	Ct Zegay	0.97	1.10	3	35.49	3	0.48	2	1.64	2	58.76	3	1.45	2	2.50	2.50	4
36	Bj Bestandji	13.35	2.01	3	91.00	3	0.45	2	2.03	2	36.24	2	1.25	2	2.33	2.33	3

No	Name																
37	Mt Bouhallouf	19.04	0.37	3	64.48	3	0.3	3	1.23	1	22.79	1	2.55	3	2.33	2.33	3
38	Dar el Oued	9.63	0.30	3	250.14	3	0.47	2	1.71	2	12.88	1	2.33	3	2.33	2.33	3
39	D Bouksaiba	7.80	0.49	3	389.88	2	0.34	3	1.46	1	23.43	1	1.62	2	2.00	2.00	3
40	Mt el Brat	21.89	1.08	3	357.35	2	0.55	1	1.46	1	15.26	1	1.85	2	1.67	1.67	2
41	Mt C.Medboh	32.16	0.33	3	129.04	3	0.29	3	2.74	2	87.17	3	0.23	1	2.50	2.50	4
42	O El Hadjar	42.83	0.26	3	130.59	3	0.31	3	1.11	1	13.35	1	2.43	3	2.33	2.33	3
43	Douar Mila	15.38	1.66	3	254.43	3	0.35	3	1.09	1	84.23	3	1.17	2	2.50	2.50	4
44	Sennaoua	14.97	3.16	2	308.36	2	0.5	1	–	–	46.08	2	4.2	3	1.67	1.67	2
45	J Kef el Arba	25.65	0.73	3	177.35	3	0.57	1	1.67	2	24.53	1	1.25	2	2.00	2.00	4
46	Didouche M.	6.80	0.49	3	97.40	3	0.26	3	1.61	2	56.63	3	1.95	2	2.67	2.67	4
47	Djebel Kellal	28.09	0.79	3	333.82	2	0.32	3	1.18	1	44.61	2	2.6	3	2.33	2.33	3
48	Mt H^{adj} Brahim	18.01	0.20	3	102.52	3	0.11	3	1.23	1	56.42	3	1.73	2	2.50	2.50	4
49	Mt H^{adj} Hamo	14.15	0.32	3	311.75	2	0.31	3	2.06	2	15.09	1	1.5	2	2.17	2.17	3
50	Mt Ali el Bana	10.15	0.23	3	130.32	3	0.3	3	1.97	2	4.34	1	0.3	1	2.17	2.17	3
51	J Akhal	114.76	1.61	3	1215	1	0.47	2	1.55	2	48.62	2	1.29	2	2.00	2.00	3
52	Constantine	45.86	1.50	3	241.24	3	0.33	3	–	–	66.14	3	0.67	1	2.17	2.17	3
53	J Agueb	41.95	1.15	3	235.43	3	0.45	2	1.73	2	56.44	3	1.2	2	2.50	2.50	4
54	J Kranga	33.62	1.10	3	120.85	1	0.3	3	2.81	3	37.62	2	1.88	2	2.67	2.67	4
55	Ibn Ziad	32.64	0.62	3	586.3	3	0.35	3	1.1	1	90.48	3	1.52	2	2.17	2.17	3
56	Ain Kerma	38.80	0.61	3	100.05	3	0.25	3	1.44	1	52.47	2	1.2	2	2.33	2.33	3
57	Beni Hamidane	18.54	1.57	3	259.7	3	0.52	1	1.35	1	53.53	2	2.48	3	2.17	2.17	3
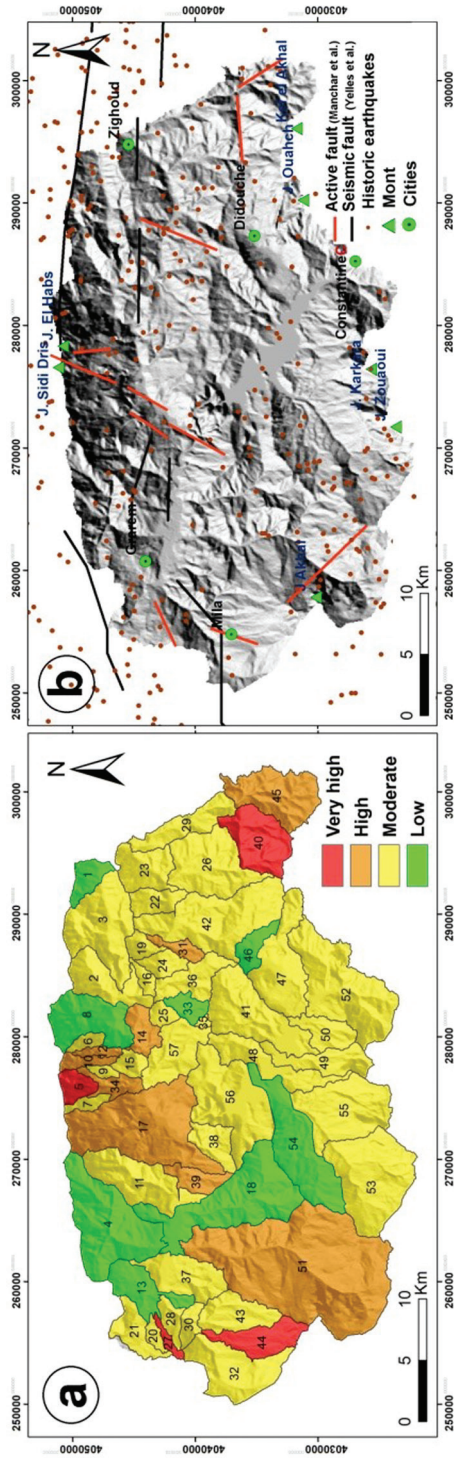
Source: Authors' own study

Fig. 6. a) relative tectonic activity indexes. b) main structure in the study area

into three classes: class one denoting high activity and class three – low activity. Iat is obtained by the standardization of the different classes of geomorphic indices (S/n). The obtained values of Iat are divided into: class 1 ($S/n < 1.5$) with very high tectonic activity; class 2 ($1.5 < S/n < 2$) with high tectonic activity; class 3 ($2 < S/n < 2.5$) with moderately active tectonics; and class 4 (of $S/n > 2.5$) with low active tectonics. Values and classess of *Bs*, *SL*, *Hi*, *Smf*, *Af*, *Vf*, and *Iat* are summarized in Table 1.

In the study area, three main structures could be identified, namely: Macheta Brat, Sidi Dris and Sennaoua-Mila. In the first structure the water flows through a main watercourse of a perfect EW linearity of NS branch until Oued Smendou (basin N° 40) shows very high tectonic activity (Fig. 6a). In the second structure, the field survey identified an NNE-SSW the sub-vertical fault of 13 km of length. This active tectonic accident separates Jurassic bedrock from the Oligo-Miocene layer. The geometry and location of the Sidi Driss fault are consistent with the spatial alignment of the earthquake clusters and the focal mechanism solutions of aftershocks [Bendjama et al. 2021]. This fault is passing through basins 05, 10, 12, 17, 14 and 34, which are classified as very high to high active tectonic (Fig. 6a). Compared to the previous results of seismological studies, such as Yelles-Chaouache et al., 2006, this research has determined new active faults speared along the Neogene basin (Fig. 6b). It was found that the main cause of the seism of Mila (07/08/2020, *Mw* = 4.9) which triggered mega landslides was related by a 4 km long NNE-SSW seismic fault in the substratum. For the main structures that have been noticed are the fault of Machetat Brat and wadi Smendou in the east; the fault of Sidi Dris to the north; the Sennaoua fault to the west; and the Jebel Akhal fault to the south. As to the NW-SE fault of Jebel Lakhal, the company responsible for digging the adduction tunnel discovered a gigantic karstic network often exceeding 2 m in height. During the first pumping tests ($Q = 23$ m³/s) numerous leaks appeared along the tunnel and could not be immediately sealed, hence the spillage of a very large quantity of water in the fractured galleries. It rushed into the faults and caused 736 small earthquakes in just 10 days [Abacha 2009]. The projection of the epicenters of the earthquakes high lighted an active SE NW fault crossing the southern flank of the Jebel Lakhal massif. The Oued Smendou strike-slip structure follows a north-south corridor, with a length of 7.5 km and a width of 3.6 km. The western boundary of the corridor reveals a series of hydrographic anomalies. While the eastern limit coincides with the abrupt changes in the directions of the wadi.

5. Conclusion and outlook perspectives

Geomorphic indices of active tectonics constitute useful parameters to assess the active tectonics in Neogene basins and their relationship with seismic activity. The values of the stream length-gradient index, along with the implication of geomorphic indices with seismic activity, in the NE of Algeria, serve as a significant tool for determining structural discontinuities and geomorphological anomalies. This method is efficient in identifying tectonically active zones. The geomorphic indices have a profound role in the landscape shaping and substratum faulting such as

the major fault of Mcid Aicha-Debagh passing behind the septentrional border of the Rhumel-Smendou subwatershed. The results obtained from *Vf* ratio shows that basins located in the North and South have a higher tectonism regime. Asymmetric factors present values of different basins, which have structural discontinuity due to passing through major faults and thrusts. Higher values of *Hi* and lower values of *Smf* suggest active erosional processes or a high degree of tectonic activity. The higher values of *Bs* and *Sl* index also defined the high degree of tectonism in the study area. All those parameters combined (determined by *Iat* parameter), and compared with seismic data and landslide susceptibility, determined the role of active tectonics in triggering landslides and other natural hazards. This study provides a tool for identifying the actual causal factors in the event of major disasters, such as landslides, earthquakes, and floods. This research requires chronological and geo-historical studies of the Holocene period. It certainly allows the characterization of the main tectonic features and the neo-formed structures.

Acknowledgements

References

Anis Z., Wissem G., Riheb H., Biswajeet P., Essghaier G.M. 2019. Effects of clay properties in the landslides genesis in flysch massif: Case study of Aïn Draham, North Western Tunisia. Journal of African Earth Sciences, 151, 146–152.

Azor A., Keller E.A., Yeats R.S. 2002. Geomorphic indicators of active fold growth: South Mountain – Oak Ridge anticline, Ventura basin, southern California. Geological Society of America Bulletin, 114(6), 745–753.

Benabbas C. 2006. Evolution Mio-Plio-Quaternaire des bassins continentaux de l'Algérie nord orientale: apport de la photogéologie et analyse morpho structurale. Thèse de doctorat, Univ. Mentouri Constantine.

Bendjama H., Yelles-Chaouche A., Boulahia O., Abacha I., Mohammedi Y., Beldjoudi H., ... Belheouane O. 2021. The March 2017 earthquake sequence along the EW-trending Mcid Aïcha-Debbagh Fault, northeast Algeria. Geosciences Journal, 25(5), 697–713.

Benmarce K., Hadji R., Zahri F., Khanchoul K., Chouabi A., Zighmi K., Hamed Y. 2021. Hydrochemical and geothermometry characterization for a geothermal system in semiarid dry climate: The case study of Hamma spring (Northeast Algeria). Journal of African Earth Sciences, 182, 104285.

Benouar D. 1994. Materials for the investigation of the seismicity of Algeria and adjacent regions during the twentieth century.

Bougrine A., Yelles-Chaouche A.K., Calais E. 2019. Active deformation in Algeria from continuous GPS measurements. Geophysical Journal International, 217(1), 572–588.

Bull W.B. 2007. Tectonic Geomorphology of Mountains: A New Approach to Paleoseismology. Blackwell, Oxford, UK.

Bull W.B., McFadden L.D. 2020. Tectonic geomorphology north and south of the Garlock fault, California. In: Geomorphology in arid regions. Routledge, 115–138.

Coiffait P.E. 1992. Un bassin post-nappe dans son cadre structural l'exemple du bassin de Constantine (Algérie Nord Orientale). Thèse en Sciences. Nancy I.P.502.

Coiffait P.E., Vila J.M. 1977. Carte géologique de l'Algérie au 1/50.000 feuille d'El Aria + notice explicative.

Dahoua L., Yakovitch S.V., Hadji R.H. 2017. GIS-based technic for roadside-slope stability assessment: an bivariate approach for A1 East-west highway, North Algeria. Mining Science, 24.

Delga M.D. 1969. Mise au point sur la structure du Nord-Est de la Berbérie.

Demdoum A., Hamed Y., Feki M., Hadji R., Djebbar M. 2015. Multi-tracer investigation of groundwater in El Eulma Basin (Northwestern Algeria), North Africa. Arabian Journal of Geosciences, 8(5), 3321–3333.

El Hamdouni R., Irigaray C., Fernández T., Chacón J., Keller E.A. 2008. Assessment of relative active tectonics, southwest border of the Sierra Nevada (southern Spain). Geomorphology, 96(1–2), 150–173.

El Mekki A., Hadji R., Chemseddine F. 2017. Use of slope failures inventory and climatic data for landslide susceptibility, vulnerability, and risk mapping in souk Ahras region. Mining Science, 24.

Guiraud R. 1973. Evolution post-triasique de l'avant-pays de la chaîne alpine en Algérie. Doctoral dissertation.

Hadji R., Limani Y., Demdoum A. 2014. Using multivariate approach and GIS applications to predict slope instability hazard case study of Machrouha municipality, NE Algeria. In: 2014 1st International Conference on Information and Communication Technologies for Disaster Management (ICT-DM). IEEE, 1–10.

Hadji R., Limani Y., Baghem M., Demdoum A. 2013. Geologic, topographic and climatic controls in landslide hazard assessment using GIS modeling: a case study of Souk Ahras region, NE Algeria. Quaternary International, 302, 224–237.

Hamad A., Hadji R., Bâali F., Houda B., Redhaounia B., Zighmi K., ... Hamed Y. 2018. Conceptual model for karstic aquifers by combined analysis of GIS, chemical, thermal, and isotopic tools in Tuniso-Algerian transboundary basin. Arabian Journal of Geosciences, 11(15), 1–16.

Hamed Y., Redhaounia B., Sâad A., Hadji R., Zahri F., Zighmi K. 2017. Hydrothermal waters from karst aquifer: Case study of the Trozza basin (Central Tunisia). Journal of Tethys, 5(1), 33–44.

Harbi A., Benouar D., Benhallou H. 2003. Re-appraisal of seismicity and seismotectonics in the north-eastern Algeria Part I: Review of historical seismicity. Journal of Seismology, 7(1), 115–136.

Hare P.W., Gardner T.W. 1985. Geomorphic indicators of vertical neotectonism along converging plate margins, Nicoya Peninsula, Costa Rica. Tectonic Geomorphology, 4, 75–104.

Keller E.A. 1986. Investigation of active tectonics: use of surficial earth processes. Active Tectonics, 1, 136–147.

Keller E.A., Pinter N. 1996. Active tectonics. Upper Saddle River, NJ, Prentice Hall, 338.

Keller E.A., Pinter N. 2002. Earthquakes, uplift, and landscape.

Mahleb A., Hadji R., Zahri F., Boudjellal R., Chibani A., Hamed Y. 2022. Water-Borne Erosion Estimation Using the Revised Universal Soil Loss Equation (RUSLE) Model Over a Semiarid Watershed: Case Study of Meskiana Catchment, Algerian-Tunisian Border. Geotechnical and Geological Engineering, 1–14.

Manchar N., Benabbas C., Bouaicha F., Boufaa K. 2019. Application of the analytical hierchy process (AHP) for landslide susceptibility mapping in the east region of Constantine, Algeria. Journal of Sciences and Technology, 4(2), 23–33.

Manchar N., Benabbas C., Hadji R., Bouaicha F., Grecu F. 2018. Landslide susceptibility assessment in Constantine region (NE Algeria) by means of statistical models. Studia Geotechnica et Mechanica, 40(3), 208–219.

McKenzie D. 1972. Active tectonics of the Mediterranean region. Geophysical Journal International, 30(2), 109–185.

Meghraoui M. 1988. Géologie des zones sismiques du Nord de l'Algérie: Paléosismologie, tectonique active et synthèse sismotectonique (doctoral dissertation, Paris 11).

Mouici R., Baali F., Hadji R., Boubaya D., Audra P., Fehdi C.É., ... Arfib B. 2017. Geophysical, Geotechnical, and Speleologic assessment for karst-sinkhole collapse genesis in Cheria plateau (NE Algeria). Mining Science, 24, 59–71.

Ncibi K., Hadji R., Hamdi M., Mokadem N., Abbes M., Khelifi F., ... Hamed Y. 2020. Application of the analytic hierarchy process to weight the criteria used to determine the Water Quality Index of groundwater in the northeastern basin of the Sidi Bouzid region, Central Tunisia. Euro-Mediterranean Journal for Environmental Integration, 5(1), 1–15.

Rais K., Kara M., Gadri L., Hadji R., Khochmen L. 2017. Original approach for the drilling process optimization in open cast mines: case study of Kef Essenoun open pit mine Northeast of Algeria. Mining Science, 24.

Ramírez-Herrera M.T. 1998. Geomorphic assessment of active tectonics in the Acambay Graben, Mexican volcanic belt. Earth Surface Processes and Landforms: The Journal of the British Geomorphological Group, 23(4), 317–332.

Raoult J.F. 1974. Géologie du centre de la chaîne numidique (nord du const, Algérie). Paris, France.

Rockwell T.K., Keller E.A., Johnson D.L. 1985. Tectonic geomorphology of alluvial fans and mountain fronts near Ventura, California. In: Tectonic Geomorphology. Proceedings of the 15th Annual Geomorphology Symposium. Allen and Unwin Publishers, Boston, MA, 183–207.

Silva P.G., Goy J.L., Zazo C., Bardajı T. 2003. Fault-generated mountain fronts in southeast Spain: geomorphologic assessment of tectonic and seismic activity. Geomorphology, 50(1–3), 203–225.

Snow R.S., Slingerland R.L. 1987. Mathematical modeling of graded river profiles. The Journal of Geology, 95(1), 15–33.

Tamani F., Hadji R., Hamad A., Hamed Y. 2019. Integrating remotely sensed and GIS data for the detailed geological mapping in semi-arid regions: case of Youks les Bains Area, Tebessa Province, NE Algeria. Geotechnical and Geological Engineering, 37(4), 2903–2913.

Vila J.M. 1980. La chaîne alpine de l'Algérie orientale et des confins algéro-tunisiens. These de Doctorat-es-sciences, Universite Pierre et Marie Curie.

Wells R.E., Weaver C.S., Blakely R.J. 1998. Fore-arc migration in Cascadia and its neotectonic significance. Geology, 26(8), 759–762.

Wildi W. 1983. La chaîne tello-rifaine (Algérie, Maroc, Tunisie): structure, stratigraphie et évolution du Trias au Miocène. Revue de géographie physique et de géologie dynamique, 24(3), 201–297.

Yelles-Chaouche A., Boudiaf A., Djellit H., Bracene R. 2006. La tectonique active de la région nord-algérienne. Comptes Rendus Geoscience, 338(1–2), 126–139.

Zahri F., Boukelloul M.L., Hadji R., Talhi K. 2016. Slope stability analysis in open pit mines of Jebel Gustar career, NE Algeria – a multi-steps approach. Mining Science, 23.

PhD Nabil Manchar
Earth Sciences, University of Oum El Bouaghi, Algeria
e-mail: manchar.nabil@univ-oeb.dz

Prof. Riheb Hadji
Department of Earth Sciences, Institute of Architecture and Earth Sciences, Ferhat Abbas University, Algeria
Laboratory of Applied Research in Engineering Geology, Geotechnics, Water Sciences, and Environment, Ferhat Abbas University, Algeria
e-mail: hadjirihab@gmail.com
ORCID: 0000-0002-9632-0812

PhD Ahmed Bougherara
Lasterne Laboratory, University of Constantine 1, Algeria
e-mail: ahbougherara@gmail.com

PhD Kamel Boufaa
LGG Laboratory, University of Jijel, Algeria
e-mail: kboufaa@hotmail.com